Ionics (2023) 29:1069–1076
https://doi.org/10.1007/s11581-022-04875-y

ORIGINAL PAPER

Fe doping modifying electronic structure of $NiSe_2$ for boosting electrocatalytic oxygen evolution reaction

Wenchang Zhuang[1] · Minglin Du[1] · Xinhua Lu[1] · Zhenyang Chen[1] · Zijun Huang[1] · Dognsheng Liu[1] · Wenjing Cheng[2] · Lin Tian[1,2]

Received: 9 November 2022 / Revised: 22 December 2022 / Accepted: 24 December 2022 / Published online: 6 January 2023

Abstract

The commercialization of hydrogen production by water electrolysis is severely hampered by the sluggish kinetics of anodic oxygen evolution reaction (OER), mainly arising from the four-electron transfer process. Electronic structure modification has been shown to be favorable for accelerating the reaction kinetics of OER by not only improving the intrinsic activity of inherent active site but also largely enhancing the electrical conductivity. Herein, we have reported a metal–organic framework (MOF)-derived strategy for the synthesis of Fe-$NiSe_2$ nanocatalysts. Upon combination of experimental data and theoretical analysis, it is reported that Fe doping can greatly modify the electronic structure of $NiSe_2$ and thus substantially promote their electrocatalytic OER performance. More importantly, it is also reported that Fe-dopant is identified as active site, meanwhile stimulating the adjacent Ni atoms as active site for OER. As a result, an overpotential of merely 277 mV is demanded for the optimal Fe-$NiSe_2$ nanocatalyst to achieve 10 mA cm^{-2} and long-term electrochemical stability for more than 35 h, which surpasses the benchmarked RuO_2 catalyst.

Keywords Doping · Electronic structure · $NiSe_2$ · Electrocatalytic oxygen evolution reaction

Introduction

Electrochemical water splitting is widely recognized as a promising technology for the storage of renewable energy and production of green and high-density hydrogen [1–3]. Although in great promise, the practical application of electrochemical water technology is greatly hampered by the intrinsically sluggish oxygen evolution reaction involved in a four-proton-coupled electron transfer process [4–7]. To date, benefitting from their low cost, environmental friendliness, high abundance, and potentially high OER activity, transition metal chalcogenides have thus been widely investigated and attracted increasing interests [8–10]. In addition, it is also reported that chalcogenides possess higher conductivity, more varied valence states and phases, and abundant redox chemistry than conventional transition metal oxides. For instance, NiSe (2630 S cm^{-1}) exhibits a few orders of magnitude higher conductivity than NiO (0.01–0.32 S cm^{-1}) [11, 12]. All of these favorable terms enabled the chalcogenides to be promising OER electrocatalyst. Among various chalcogenides, Ni-selenides have been confirmed to be potential OER catalyst due to the suitable adsorption energy of various intermediates and adjustable electronic structure [13, 14]. For an update, the best Ni-selenides reported so far can deliver a current density of 10 mA cm^{-2} with the overpotential lower than 250 mV [15, 16]. However, most of the Ni-selenides delivers an overpotential of at least 300 mV [17], and furthermore, a current stability was maintained for only dozens of hours, letting alone a high current density for thousands of hours. One of the major obstacles that limit their catalytic activity is the non-optimized electronic structure for electron transfer and the adsorption/desorption of OER intermediates [18, 19]. Therefore, tuning or creating an optimal electronic structure of Ni-selenides will benefit for the substantial improvement in electrocatalytic OER performance [20, 21].

In recent years, many effective strategies have been proposed for tuning the electronic structure [22, 23]. Among

✉ Lin Tian
xzittl@xzit.edu.cn

[1] School of Materials and Chemical Engineering, Xuzhou University of Technology, Xuzhou 221018, People's Republic of China

[2] School of Chemistry and Environmental Science, Yili Normal University, Yili 835000, People's Republic of China

them, heteroatom doping is reported to be a highly effective method of realizing the electronic structure regulation [24, 25]. According to the *d*-band center theory, the adsorption energy of oxygen intermediates could be flexibly tuned by heteroatom doping [26, 27]. For example, Ta doping can induce the lattice expansion of layered double hydroxide (LDH) and modify electronic structure through electron transfer from Fe to Ta [28]. Also, the modified electronic structure among Ni, Fe, and Ta and the modified e_g orbital of Ta induced by charge transfer also benefit for the adsorption of OH species on Ta site in Ta-doped NiFe LDH and increase the intrinsic metallic property of NiFe LDH. In addition, it is also demonstrated that heteroatom doping can also activate the adjacent metal atoms to further improve the intrinsically OER activity [29]. More importantly, excepting for optimizing the binding strengths with oxygen intermediates, it is demonstrated that heteroatom doping can also substantially suppress the dissolution of the electrocatalyst during long-term electrochemical operation [30].

By taking considerations of the intrinsically high activity of Ni-selenides and positive influences of heteroatom doping on the optimization of electronic structure, we herein reported the synthesis of Fe-doped $NiSe_2$ nanocatalysts via a simple MOF-derived strategy. Importantly, the optimal Fe-$NiSe_2$-6 catalyst can achieve a current density of 10 mA cm^{-2} with the overpotential of 277 mV. Inspiringly, the water-alkali electrolyze of Fe-$NiSe_2$-6 || Pt/C exhibited a low cell voltage of 1.57 V to reach 10 mA cm^{-2} and excellent durability for at least 30 h. By combining the experimental data and theoretical study, it is demonstrated that the electronic structure optimization of Ni after Fe doping predominantly contributes to the substantial improvement in electrocatalytic OER activity and therefore provides a better understanding on the key importance of electronic structure engineering for the promotion of OER activity.

Experimental section

Preparation of NiFe-MOF-74

NiFe-MOF-74 were prepared by a facile solvothermal based on previous report [31]. Typically, 90 mg 2,5-dihydroxytelephthalic acid, 157 mg nickel nitrate hexahydrate ($Ni(NO_3)_2{\cdot}6H_2O$), and 15.7 mg ferrous acetate ($Fe{\cdot}(C_2H_3O_2)_2$) were poured into the mixed solution of 30 mL DMF, 1.8 mL ethanol, and 1.8 mL DI water. After 30 min of sonication, the mixture was transferred into a 100-mL Teflon-lined stainless autoclave for keeping reaction at 120 °C for 24 h. After cooling to room temperature, the NiFe-MOF-74(6:1) were obtained by centrifugation and washed with methanol and ethanol for several. For comparison, the Ni-MOF, NiFe-MOF-74(3:1) and NiFe-MOF-74(9:1) were also prepared by only tuning the content of $Fe{\cdot}(C_2H_3O_2)_2$ to 0 mg, 31.4 mg, and 10.4 mg, respectively.

Preparation of Fe-$NiSe_2$

Ten milligrams of NiFe-MOF-74(6:1) was dispersed into 5 mL DI water, 1 mL aqueous solution with 12 mg SeO_2 was also added into the above solution, and subsequently, 0.1 mL $N_2H_4{\cdot}H_2O$ was dropped into the mixture. After stirring for 10 min, the mixture was poured into a 30-mL Teflon-lined stainless autoclave to maintain for 8 h at 160 °C. After cooling to room temperature, the product Fe-$NiSe_2$-6 was collected through centrifugation and washed with DI water.

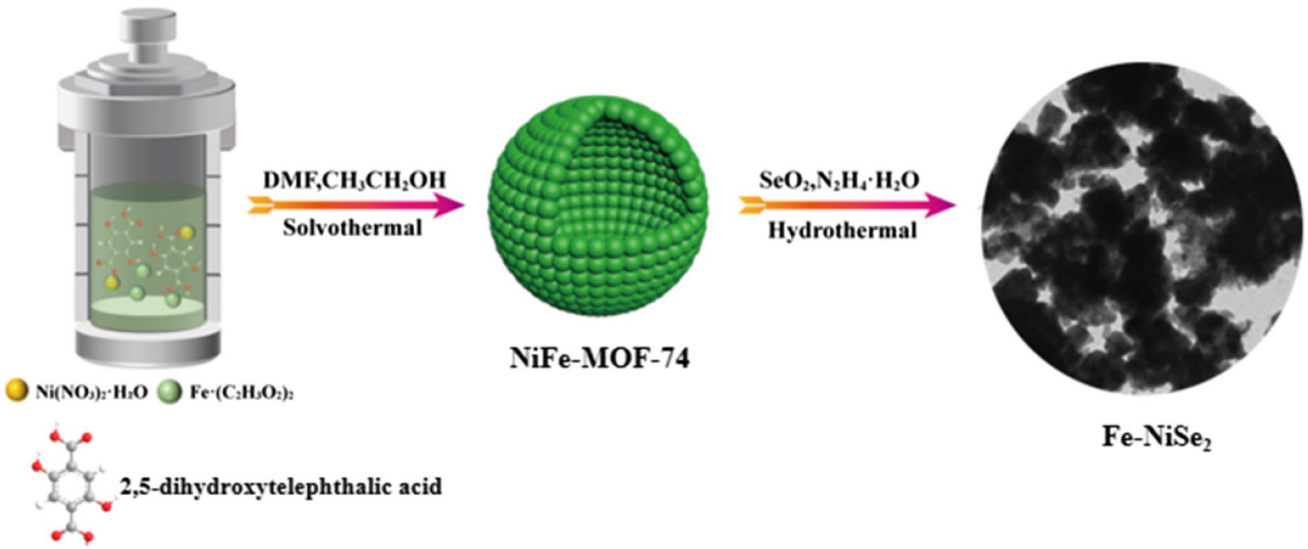

Fig. 1 The scheme for the synthesis of Fe-NiSe2

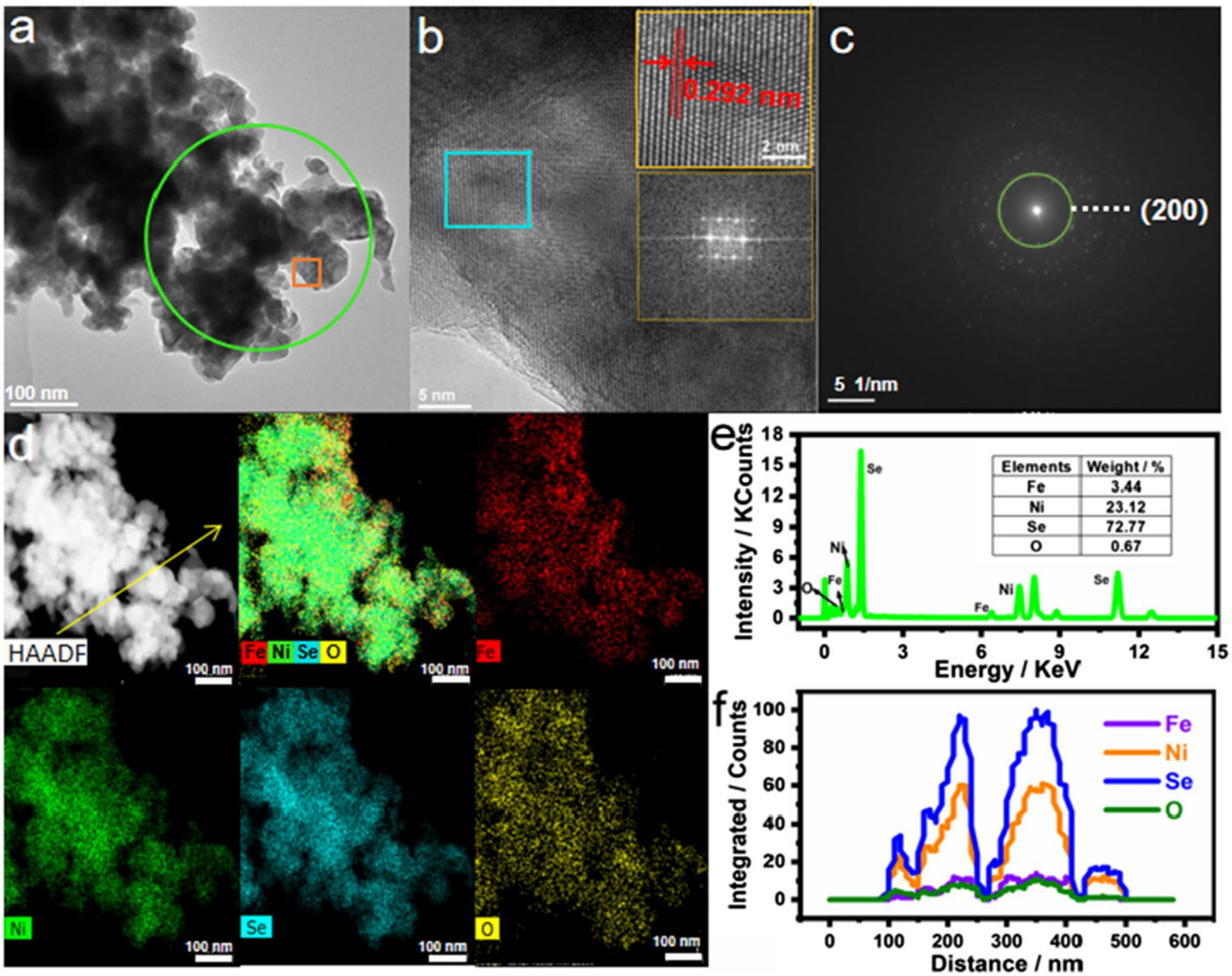

Fig. 2 a TEM image of Fe-NiSe2; b HRTEM images (orange area in a), inset images represents the corresponding HRTEM of area and FFT patterns of selected areas of fresh green box; c SAED pattern (corresponding the fresh green area in a); d STEM image and the corresponding elemental mapping images of Fe, Ni, Se, and O in Fe-NiSe2-6; e EDS spectrum of Fe-NiSe2-6; f the compositional line profile highlighted in yellow line

Characterizations

The phase and structure of all the samples were confirmed by powder X-ray diffraction (XRD, Rigaku UIV, Japan). The morphology of the samples was observed on scanning electron microscopy (TEM, JEOL-2100, Japan). The valence states and composition of surface elements in the samples were explored by X-ray photoelectron spectroscopy (XPS, JEOL JPS-9010 MC, Japan).

Electrochemical measurements

The standard three-electrode system, which equipped with modified glass carbon electrode, Ag/AgCl electrode, and carbon rod as working electrode, reference electrode, and counter electrode, respectively, was applied to evaluate their electrocatalytic performance with a CHI-760E electrochemical workstation. Linear sweep voltammetry (LSV) was obtained at the scan rate of 5 $mV{\cdot}s^{-1}$. Capacitance (C_{dl}) was calculated with assistance of cyclic voltammetry (CV) in a non-faradaic region at 10, 20, 50, 100, and 200 $mV{\cdot}s^{-1}$, respectively. The electrochemical impedance spectroscopy (EIS) was performed from 1 Hz to 1000 kHz with a sinusoidal perturbation of 0.5 mA. The chronopotentiometry (CP) test was continuously carried out at a constant current density of 10 mA cm^{-2}.

Results and discussion

As illustrated in Fig. 1, the synthesis of Fe-$NiSe_2$ involved two steps, where the NiFe-MOF-74 can be synthesized via a simple solvothermal method by employing $Ni(NO_3)_2{\cdot}6H_2O$

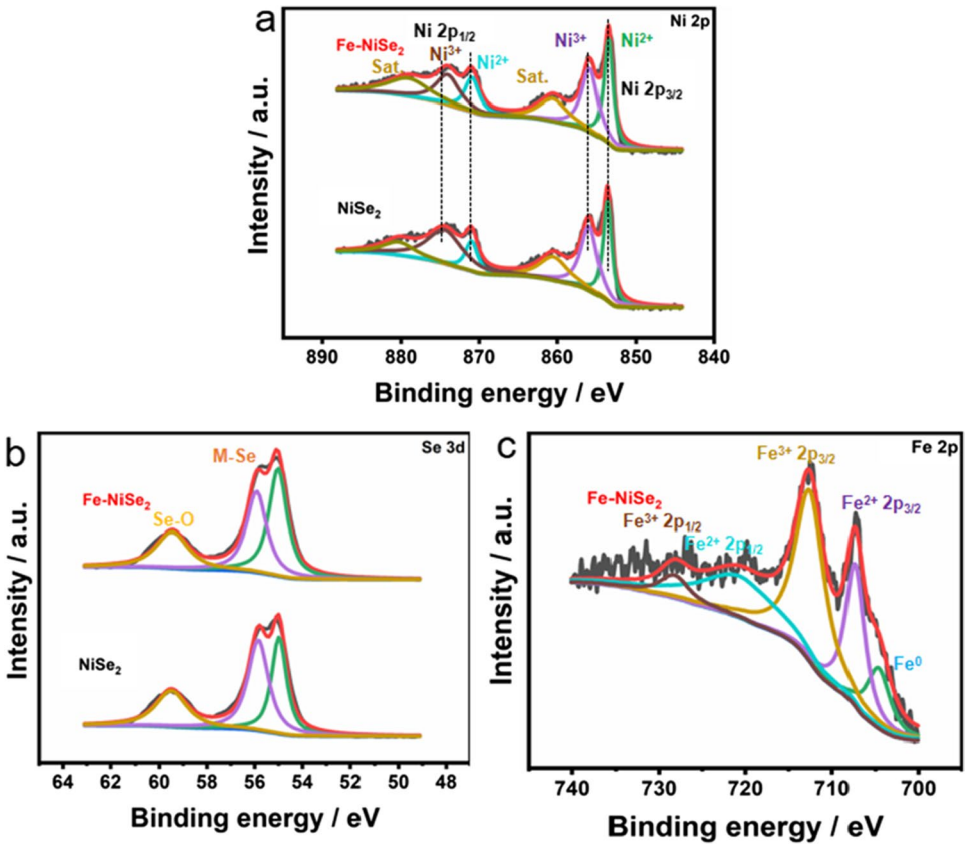

Fig. 3 The high-resolution XPS spectra of a Ni 2p, b Se 3d, and c Fe 2p

and Fe·$(C_2H_3O_2)_2$ as precursors, DMF, and CH_2CH_2OH as solvent. Interestingly, the morphology of the NiFe-MOF-74 is varied by changing the molar ratio of $Ni(NO_3)_2{\cdot}6H_2O$ and Fe·$(C_2H_3O_2)_2$. As shown in Fig. S1a, the pristine Ni-MOF-74 is featured with typical sphere-like morphology. When varying the molar ratio of $Ni(NO_3)_2{\cdot}6H_2O$ and Fe·$(C_2H_3O_2)_2$ from 3:1 to 6:1 and 9:1, the morphology is changed into spinning conical (Fig. S1b), hollow nanosphere (Fig. S1c), and nanoflower (Fig. S1d), respectively [32, 33]. Then, the Fe-$NiSe_2$ can be obtained via a simple hydrothermal method using NiFe-MOF-74 as precursors and SeO_2 as Se source.

To catch the morphological and structural information of the as-prepared Fe-$NiSe_2$ catalyst, a series of morphology and structure characterizations have also been conducted. The TEM image in the Fig. 2a implied that the as-prepared Fe-$NiSe_2$ are featured with porous properties, which will benefit for charge transfer efficiency and mass transport for electrocatalysis. The HRTEM image in Fig. 2b indicated the high crystallinity of Fe-$NiSe_2$, in which the *d*-spacing of 0.292 nm can be indexed to the (200) facet of Fe-$NiSe_2$, being consistent with the analysis of SAED pattern (Fig. 2c). The XRD peaks of Fe-$NiSe_2$ can be well indexed to the $NiSe_2$ (JCPDS# 41–1495) except for the slight shift due to the larger atomic radius of Fe, while some weak diffraction peaks can be assigned to the $NiSe_2$ (JCPDS# 21–0432) (Fig. S2) [34]. Besides the morphology and structure, the chemical composition of the Fe-$NiSe_2$ is also thoroughly investigated. Figure 2d showed the EDS elemental mapping images of the Fe-$NiSe_2$ catalyst, where the Fe, Ni, and Se elements are homogeneously dispersed throughout the nanostructure, indicating the successful fabrication of Fe-$NiSe_2$ catalyst. The EDS spectrum (Fig. 2e) and line-scan profile (Fig. 2f) also suggested the successful doping of Fe into $NiSe_2$, with a percentage of 3.44%. The abundant O element is observed in the EDS spectrum of Fe-$NiSe_2$, maybe originated from the oxygen adsorbed on the surface of the material and oxygen contained in surface functional groups.

The valence state and compositions of the Fe-$NiSe_2$ were also analyzed by XPS by using $NiSe_2$ as a referenced sample. The survey spectra revealed the occurrence of C, Ni, Fe, and Se elements and trace amount of O from air exposure (Fig. S3). The Ni 2p XPS spectrum featured two twist circles of Ni $2p_{3/2}$ and Ni $2p_{1/2}$ connected by two associative satellite peaks (Fig. 3a). Both the peaks for Ni $2p_{3/2}$ and Ni $2p_{1/2}$ can be assigned to the Ni^{2+} and Ni^{3+}. Interestingly, when compared with $NiSe_2$, the Ni 2p spectrum of Fe-$NiSe_2$ can display a slight shift to lower binding energy, suggesting that the dopant of trace amount of Fe can induce the charge transfer, which is indirectly indicating the Fe doping can modify the electronic structure of $NiSe_2$ [35, 36]. The Se 3d can also fitted to the Se^{2-} of $3d_{5/2}$ and $3d_{3/2}$, respectively (Fig. 3b), indicating the

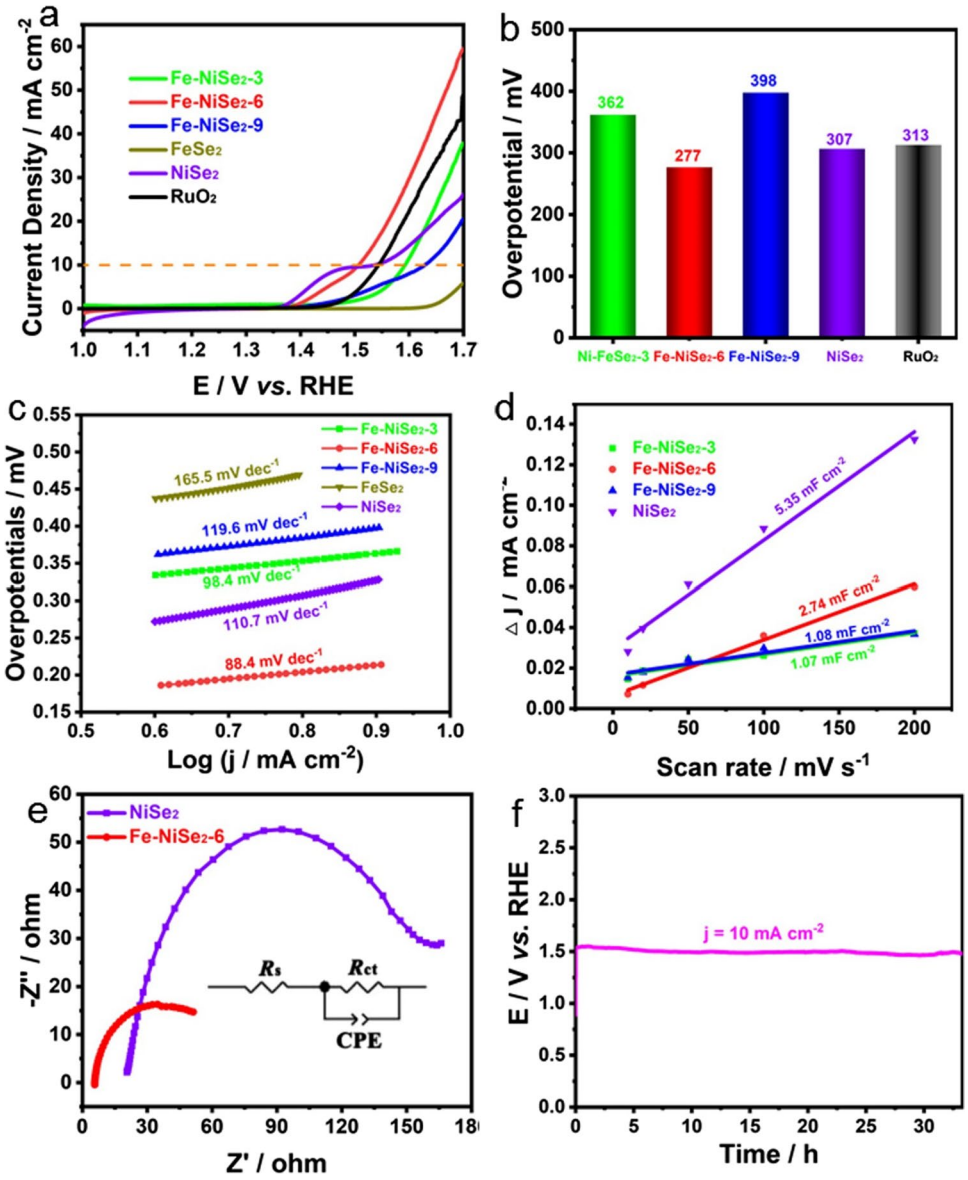

Fig. 4 a LSV polarization curves of Fe-NiSe2-3, Fe-NiSe2-6, Fe-NiSe2-9, FeSe2, NiSe2, and RuO2. b Histograms of the overpotentials of different products at 10 mA cm-2. c Tafel plots of different electrocatalysts. d Current density as a function of the scan rate for the different electrodes. e Nyquist plots of different products at 0.5 V. f The prolonged CP of Fe-NiSe2 at a current density of 10 mA cm-2

formation of Ni-Se [37]. Furthermore, we also find the XPS spectra of Se before Fe doping is similar with the spectrum after Fe doping. For Fe 2p (Fig. 3c), the peaks appeared at the binding energies around 707.5 eV and 721.2 eV were compatible with Fe^{2+} $2p_{3/2}$ and Fe^{2+} $2p_{1/2}$, respectively, while the other two peaks presented at the binding energies around 712.7 eV and 728.6 eV were well indexed to the Fe^{3+} $2p_{3/2}$ and Fe^{3+} $2p_{1/2}$, respectively [38]. According to the XPS analysis, it is concluded that the negative shift of Ni 2p suggests the electron transfer from Fe to Ni, suggesting Fe doping can effectively tailor the electronic structure of nickel [39].

The electrocatalytic OER performance of the Fe-$NiSe_2$ was evaluated in 1 M KOH electrolyze by benchmarking $FeSe_2$, $NiSe_2$, and RuO_2. For comparison, the Fe-$NiSe_2$ with different Ni/Fe ratios are also synthesized and evaluated. As shown in Fig. S4, both the Fe-$NiSe_2$-3 and Fe-$NiSe_2$-9 can also exhibit the coral morphology similar to Fe-$NiSe_2$-6, suggesting this method is universal for the synthesis of a series of Fe-$NiSe_2$ nanocatalysts with adjustable Ni/Fe atomic ratio. Figure 4a showed the LSV polarization curves of different electrocatalysts in 1 M KOH solution with a scan rate of 5 mV s^{-1}. As shown in Fig. 4a, it is clearly observed that the Fe-$NiSe_2$-6 can deliver remarkably higher current density and lower onset potential than other electrocatalysts. As seen from Fig. S5, an onset potential of merely 1.39 V is demanded for Fe-$NiSe_2$-6 to drive electrocatalytic water oxidation, being much smaller than

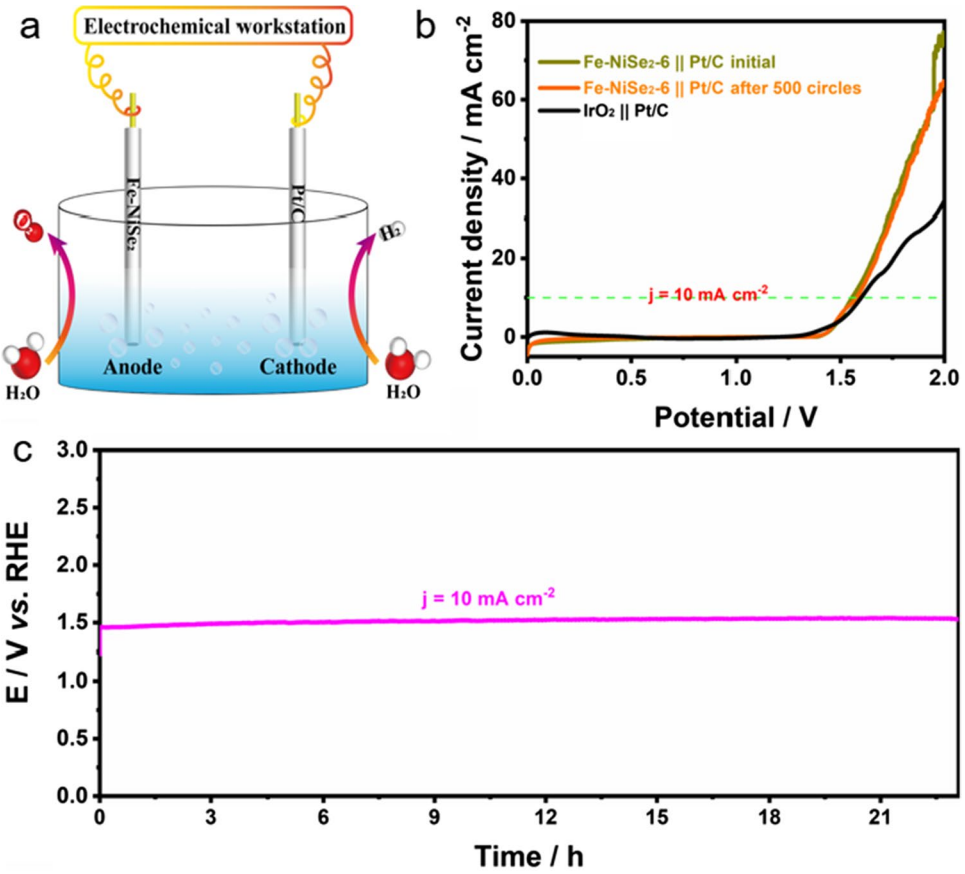

Fig. 5 a Schematically presenting the electrochemical overall water splitting based on Fe-NiSe2-6||Pt/C couple. b LSV polarization curves of Fe-NiSe2-6||Pt/C and RuO2||Pt/C toward water electrolysis. c The long-time CP curve of Fe-NiSe2-6||Pt/C couple at 10 mA cm-2

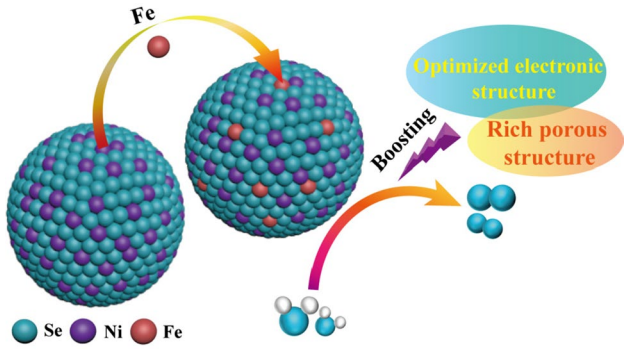

Fig. 6 Improving mechanism of the electrocatalytic OER performance of Fe-$NiSe_2$

other electrocatalysts. For systematically comparing the OER activity of different catalysts, a histogram of the overpotentials of different electrocatalysts at 10 mA cm^{-2} is summarized in Fig. 4b. As shown in Fig. 4b, it is clearly observed that the Fe-$NiSe_2$-6 can archive 10 mA cm^{-2} with the overpotential of only 277 mV, which is the smallest among these electrocatalysts investigated and surpass more reported Fe-$NiSe_2$ OER electrocatalysts [40]. In order to investigate the influence of the electronic structure optimization on the reaction kinetics of OER, we have calculated the Tafel slope of different electrocatalysts. As displayed in Fig. 4c, the Tafel slope of Fe-$NiSe_2$-6 is 88.4 mV dec^{-1}, which is much smaller than that of $FeSe_2$ and $NiSe_2$. In addition, both the Fe-$NiSe_2$-3 and Fe-$NiSe_2$-9 can also exhibit much smaller Tafel slope than that of $FeSe_2$ and $NiSe_2$, further implying the positive influence of the electronic structure optimization on the acceleration of reaction kinetics [41]. The electrochemical active surface areas of these electrocatalysts are further evaluated by electrochemical double-layer capacitance (Fig. 4d). Herein, the capacitance of Fe-$NiSe_2$-6 is as high as 2.74 mF cm^{-2}, suggesting abundant electrochemically active sites are available for oxygen intermediates. To evaluate the electron transfer capability of Fe-$NiSe_2$-6, the electrochemical impedance spectra are also obtained, where the Fe-$NiSe_2$-6 shows a remarkably smaller impedance arc diameter than $NiSe_2$ (Fig. 4e), suggesting the high electrical conductivity and good electron transfer capability [42]. Besides the electrochemical activity, catalytic stability is also crucial for the practical application of electrocatalyst. To this end, we have thus carried out a chronopotentiometry (CP) test to evaluate the electrochemical stability. As shown in Fig. 4f, the Fe-$NiSe_2$-6 can run stably over 35 h at a current density of 10 mA cm^{-2} without amplification in overpotential. The negligible variation in overpotential further confirm its superb electrochemical stability [43].

To investigate the potential for driving electrochemical overall water splitting, a two-electrode water electrolysis system equipped by Fe-$NiSe_2$ as anode and Pt/C as cathode is assembled (Fig. 5a). As shown in Fig. 5b, the Fe-$NiSe_2$-6 || Pt/C electrode exhibited obviously higher current density than that of the IrO_2 || Pt/C electrode, which requires a cell voltage of only 1.57 V to deliver a current density of 10 mA cm^{-2}. More importantly, the LSV polarization curve after 500 potential CV cycles is almost overlapped with the initial one, suggesting the high electrochemical durability for overall water splitting. More importantly, this couple can also exhibit superb voltage stability by maintaining a stable cell potential at the current density of 10 mA cm^{-2} without obvious amplification for more than 25 h (Fig. 5c). These electrochemical tests have further indicated the great potential of Fe-$NiSe_2$-6 for the practical application in driving electrochemical water splitting (Fig. 6) [44].

Upon the combination of characterizations and electrochemical tests, it is concluded that the outstanding electrocatalytic OER performance of the Fe-$NiSe_2$ is primarily attributed to the electronic structure modification after Fe doping, which greatly optimizes the binding strength with oxygen intermediates [45]. Moreover, the porous structure also contributes to the substantial improvement in OER activity and stability [46, 47].

Conclusion

In summary, a MOF-derived strategy has been proposed for the fabrication of Fe-$NiSe_2$ with modified electronic structure and porous architecture. It is demonstrated that a trace amount of Fe doping can greatly modulate the electronic structure of $NiSe_2$, enabling them to possess an optimized binding strength with oxygen intermediates. Moreover, the porous structure can also expose more accessible active sites for intermediates. Benefitting from the modulated electronic structure and porous architecture, such Fe-$NiSe_2$ can exhibit superb catalytic OER performance with an overpotential of 277 mV at 10 mA cm^{-2}, and a Tafel slope of 46.3 mV dec^{-1} in 1.0 M KOH, as well as remarkably high cycle stability. This work demonstrated the power of electronic structure engineering in designing advanced OER electrocatalysts with super catalytic activity, and it is highly anticipated that more work on electronic structure engineering of other potential materials may be stimulated.

Supplementary Information The online version contains supplementary material available at https://doi.org/10.1007/s11581-022-04875-y.

Funding This work was financed by the Xuzhou Science and Technology Plan Project of China (KC21294).

References

1. Wang ZP, Xiao BB, Lin ZP et al (2021) $PtSe_2$/Pt heterointerface with reduced coordination for boosted hydrogen evolution reaction. Angew Chem Int Ed 60(43):23388–23393
2. Xu H, Yuan J, He G, Chen H (2023) Current and future trends for spinel-type electrocatalysts in electrocatalytic oxygen evolution reaction. Coord Chem Rev 475:214869
3. Wang ZP, Lin ZP, Deng J et al (2021) Elevating the d-band center of six-coordinated octahedrons in Co_9S_8 through Fe-incorporated topochemical deintercalation. Adv Energy Mater 11:2003023
4. Du Y, Cheng G, Luo W et al (2017) Colloidal synthesis of urchin-like Fe doped $NiSe_2$ for efficient oxygen evolution. Nanoscale 9(20):6821–6825
5. Li Z, Liu D, Lu X, Du M, Chen Z, Teng J et al (2022) Boosting oxygen evolution of layered double hydroxide through electronic coupling with ultralow noble metal doping. Dalton Trans 51:1527–1532
6. Wang ZP, Xiao BB, Lin ZP et al (2021) In-situ surface decoration of RuO_2 nanoparticles by laser ablation for improved oxygen evolution reaction activity in both acid and alkali solutions. J Energy Chem 54:510–518
7. Gu X, Liu Z, Li H et al (2021) Fluorination of ZIF-67 framework templated Prussian blue analogue nano-box for efficient electrochemical oxygen evolution reaction. Chem Eng J 403:126371
8. Lin ZP, Wang ZP, Shen SJ et al (2020) One-step method to achieve multiple decorations on lamellar MoS_2 to synergistically enhance the electrocatalytic HER performance. J Alloys Compds 834:155217
9. Lin ZP, Lin B, Wang ZP et al (2019) Facile preparation of 1T-$Mo(S_{1-x}Se_x)_2$ nanoparticles for boosting hydrogen evolution reaction. ChemCatChem 11(8):2217–2222
10. Lin ZP, Wang CW, Wang ZP et al (2018) The role of conductivity and phase structure in enhancing catalytic activity of CoSe for hydrogen evolution reaction. Electrochim Acta 294:142–147
11. Tian L, Chen H, Lu X, Liu D, Cheng W, Liu Y et al (2022) Local photothermal and photoelectric effect synergistically boost hollow CeO_2/CoS_2 heterostructure electrocatalytic oxygen evolution reaction. J Colloid Interface Sci 628:663–672
12. Li X, Han GQ, Liu YR et al (2016) NiSe@NiOOH core-shell hyacinth-like nanostructures on nickel foam synthesized by in situ electrochemical oxidation as an efficient electrocatalyst for the oxygen evolution reaction. ACS Appl Mater Interfaces 8(31):20057–20066
13. Li Y, Yan D, Zou Y et al (2017) Rapidly engineering the electronic properties and morphological structure of NiSe nanowires for the oxygen evolution reaction. J Mater Chem A 5(48):25494–25500
14. Bao WW, Yang CM, Ai TT et al (2023) Modulating interfacial charge distribution of NiSe nanoarrays with NiFe-LDH nanosheets for boosting oxygen evolution reaction. Fuel 332:126227
15. Gu C, Hu S, Zheng X et al (2018) Synthesis of Sub-2 nm Fe-Doped NiSe2 nanowires and their surface confined oxidation for oxygen evolution catalysis. Angew Chem Int Ed 130(15):4084–4088
16. Li Z, Xu X, Lu X et al (2022) Synergistic coupling of $FeNi_3$ alloy with graphene carbon dots for advanced oxygen evolution reaction electrocatalysis. J Colloid Interface Sci 615:273–281
17. Liu T, Ma X, Liu D et al (2016) Mn doping of CoP nanosheets array: an efficient electrocatalyst for hydrogen evolution reaction with enhanced activity at all pH values. ACS Catal 7(1):98–102

18. Niu S, Jiang WJ, Wei Z et al (2019) Se-doping activates FeOOH for cost-effective and efficient electrochemical water oxidation. J Am Chem Soc 141(17):7005–7013
19. Peng S, Gong F, Li L et al (2018) Necklace-like multishelled hollow spinel oxides with oxygen vacancies for efficient water electrolysis. J Am Chem Soc 140(42):13644–13653
20. Rubio-Giménez V, Waerenborgh JC, Clemente-Juan JM (2017) Spontaneous magnetization in heterometallic NiFe-MOF-74 microporous magnets by controlled iron doping. Chem Mater 29(15):6181–6185
21. Shen X, Zhang M, Sudi MS et al (2021) Synergistic optimization promoted overall water splitting of CoSe@$NiSe_2$@MoS_2 heterostructured composites. Chem Commun (Camb) 57(93):12516–12519
22. Sun Y, Xue Z, Liu Q, Jia Y, Li Y, Liu K et al (2021) Modulating electronic structure of metal-organic frameworks by introducing atomically dispersed Ru for efficient hydrogen evolution. Nat Commun 12(1):1369
23. Zhang JJ, Li MY, Li X (2022) Chromium-modified ultrathin CoFe LDH as high-efficiency electrode for hydrogen evolution reaction. Nanomater 12:1227
24. Tian L, Li Z, Xu X (2021) Advances in noble metal (Ru, Rh, and Ir) doping for boosting water splitting electrocatalysis. J Mater Chem A 9(23):13459–13470
25. Wang Q, Huang X, Zhao ZL et al (2020) Ultrahigh-loading of Ir single atoms on NiO matrix to dramatically enhance oxygen evolution reaction. J Am Chem Soc 142(16):7425–7433
26. Wang Q, Zhang Z, Cai C et al (2021) Single iridium atom doped Ni_2P catalyst for optimal oxygen evolution. J Am Chem Soc 143(34):13605–13615
27. Wang S, Zhao L, Li J (2022) High valence state of Ni and Mo synergism in NiS_2-MoS_2 hetero-nanorods catalyst with layered surface structure for urea electrocatalysis. J Energy Chem 66:483–492
28. Wang X, Tuo Y, Zhou Y (2021) Ta-doping triggered electronic structural engineering and strain effect in NiFe LDH for enhanced water oxidation. Chem Eng J 403:126297
29. Wu ZP, Zhang H, Zuo S et al (2021) Manipulating the local coordination and electronic structures for efficient electrocatalytic oxygen evolution. Adv Mater 33(40):e2103004
30. Xiong Q, Wang Y, Liu PF et al (2018) Cobalt covalent doping in MoS_2 to Induce bifunctionality of overall water splitting. Adv Mater 30(29):e1801450
31. Yin J, Jin J, Zhang H et al (2019) Atomic arrangement in metal doped NiS_2 boosts hydrogen evolution reaction in alkaline media. Angew Chem Int Ed 131(51):18849–18855
32. Xu C, Li Q, Shen J et al (2019) A facile sequential ion exchange strategy to synthesize $CoSe_2$/$FeSe_2$ double-shelled hollow nanocuboids for the highly active and stable oxygen evolution reaction. Nanoscale 11(22):10738–10745
33. Xu H, Huang B, Zhao Y et al (2022) Engineering heterostructured Pd-Bi_2Te_3 doughnut/Pd hollow nanospheres for ethylene glycol electrooxidation. Inorg Chem 61(10):4533–4540
34. Xu B, Chen Z, Yang X et al (2018) Electronic modulation of carbon-encapsulated NiSe composites via Fe doping for synergistic oxygen evolution. Chem Commun (Camb) 54(65):9075–9078
35. Xu H, Shang H, Wang C et al (2020) Surface and interface engineering of noble-metal-free electrocatalysts for efficient overall water splitting. Coord Chem Rev 418:213374
36. Xiao L, Bao WW, Zhang JJ et al (2022) Interfacial interaction between NiMoP and NiFe-LDH to regulate the electronic structure toward high-efficiency electrocatalytic oxygen evolutionreaction. Int J Hydrogen Energy 47:9230–9238
37. Li Z, Jiang ZZ, Zhu WJ et al (2020) Facile preparation of $CoSe_2$ nano-vesicle derived from ZIF-67 and their application for efficient water oxidation. Appl Surf Sci 504:144368
38. Tian L, Pang X, Xu H, Liu D, Lu X, Li J et al (2022) Cation-anion dual doping modifying electronic structure of hollow CoP nanoboxes for enhanced water oxidation electrocatalysis. Inorg Chem 61:16944–16951
39. Xu H, Zhao Y, Wang Q et al (2022) Supports promote single-atom catalysts toward advanced electrocatalysis. Coord Chem Rev 451:214267
40. Zhou J, Yuan LW, Wang JW et al (2020) Combinational modulations of NiSe2 nanodendrites by phase engineering and irondoping towards an efficient oxygen evolution reaction. J Mater Chem A 8:8113
41. Tian L, Huang Z, Na W, Liu Y, Wang S, He Y et al (2022) The heterojunction MnO_2 nanosheet decorated Ag nanowires with enhanced oxidase-like activity for sensitively dual-mode detection of glutathione. Nanoscale 14:15340
42. Xu H, Wang C, He G et al (2022) Hierarchical hollow $CoWO_4$-$Co(OH)_2$ heterostructured nanoboxes enabling efficient water oxidation electrocatalysis. Inorg Chem 61(35):14224
43. Zhang Q, Wang K, Zhang M et al (2022) Electronic structure optimization boosts Pd nanocrystals for ethanol electrooxidation realized by Te doping. CrystEngComm 24(31):5580–5587
44. Yin J, Jing J, Lu M et al (2020) Iridium single atoms coupling with oxygen vacancies boosts oxygen evolution reaction in acid media. J Am Chem Soc 142:18378
45. Zheng X, Han X, Cao Y et al (2020) Identifying dense $NiSe_2$/$CoSe_2$ heterointerfaces coupled with surface high-valence bimetallic sites for synergistically enhanced oxygen electrocatalysis. Adv Mater 32(26):e2000607
46. Tian L, Liu Y, He C, Tang S, Li J, Li Z (2022) Hollow heterostructured nanocatalysts for boosting electrocatalytic water splitting. Chem Rec e202200213
47. Tian L, Chen Z, Wang T, Cao M, Lu X, Cheng W et al (2023) Mo doping and Se vacancy engineering for boosting electrocatalytic water oxidation by regulating the electronic structure of self-supported Co9Se8@NiSe. Nanoscale 15:259